Mathematical Modelling and Analysis
Volume 29, Issue 4, 714–730, 2024
https://doi.org/10.3846/mma.2024.20646

A Two-Derivative Time Integrator for the Cahn-Hilliard Equation

Eleni Theodosiou[a], Carina Bringedal[b] and Jochen Schütz[a]

[a] *Faculty of Sciences & Data Science Institute, Hasselt University*
Agoralaan Gebouw D, 3590 Diepenbeek, Belgium
[b] *Department of Computer Science, Electrical Engineering and Mathematical Sciences, Western Norway University of Applied Sciences*
Inndalsveien 28, 5063 Bergen, Norway
E-mail(*corresp.*): eleni.theodosiou@uhasselt.be
E-mail: carina.bringedal@hvl.no
E-mail: jochen.schuetz@uhasselt.be

Received December 19, 2023; accepted April 26, 2024

Abstract. This paper presents a two-derivative energy-stable method for the Cahn-Hilliard equation. We use a fully implicit time discretization with the addition of two stabilization terms to maintain the energy stability. As far as we know, this is the first time an energy-stable multiderivative method has been developed for phase-field models. We present numerical results of the novel method to support our mathematical analysis. In addition, we perform numerical experiments of two multiderivative predictor-corrector methods of fourth and sixth-order accuracy, and we show numerically that all the methods are energy stable.

Keywords: multiderivative methods, high-order methods, Cahn-Hilliard equation, energy-stable methods.

AMS Subject Classification: 65L07; 65L20; 35Q35.

1 Introduction

In this work, we consider the numerical integration of the Cahn-Hilliard [6] (CH) equation describing phase separation in multiphase flow, see, e.g., [2, 3, 4, 5, 8, 14, 20, 21, 24, 34, 38] and the references therein. The equations are given

through

$$\begin{aligned} u_t &= \Delta\mu, && (x,t) \in \Omega \times (0, T_{\text{end}}), \\ \mu &= \Phi'(u) - \varepsilon^2 \Delta u, && (x,t) \in \Omega \times (0, T_{\text{end}}), \end{aligned} \tag{1.1}$$

for some bounded domain $\Omega \in \mathbb{R}^d$ and $T_{\text{end}} \in \mathbb{R}^+$, subject to Neumann boundary conditions on the boundary $\partial\Omega$ for both the phase field u and the potential μ, i.e.,

$$\nabla u \cdot n = \nabla \mu \cdot n = 0, \quad (x,t) \in \partial\Omega \times (0, T_{\text{end}}).$$

Additionally we have an initial condition u_0 for u at time $t = 0$. In this work, we assume that the free energy $\Phi(u)$ is a double-well potential [23], i.e.,

$$\Phi(u) := \frac{1}{4}(u^2 - 1)^2.$$

Note that ε is a small, yet finite positive number. The Cahn-Hilliard equation (1.1) is inherently stiff. This is mostly due to fact that, when written in primal form, it contains a fourth-order spatial derivative, and a nonlinear free-energy density function. In addition, Cahn-Hilliard equation suffers from steep gradients. This in practice leads to very harsh restrictions on the time-step size Δt for explicit schemes, which can be as worse as $\Delta t = \mathcal{O}(\Delta x^4)$ [17], where Δx is the characteristic length of a spatial element. Hence, in this work, we focus on *implicit* time integration schemes for Equation (1.1).

In particular, we focus on the class of two-derivative methods in this work, see e.g., [1, 18, 19, 25, 28, 29]. The fundamental idea behind those methods is to not only account for the first temporal derivative of an ordinary differential equation (ODE) – which is the flux – but also of the second temporal derivative. To put the ideas more into context, assume that an ODE is given by

$$u'(t) = Q(u(t)),$$

where $Q : \mathbb{R}^m \to \mathbb{R}^m$ is a smooth flux function; and here in this context could denote a spatial discretization of (1.1). It is straightforward to show that

$$u''(t) = Q'(u)Q(u) =: Q^{(2)}(u),$$

(to avoid a clumsy notation, we refrain from writing the t-dependency explicitly each time). If the function $Q^{(2)}$ is included in a time-marching scheme, one obtains a two-derivative scheme. A classical example that we treat in this work is the implicit second-order Taylor scheme

$$u^{n+1} = u^n + \Delta t Q(u^{n+1}) - \frac{\Delta t^2}{2} Q^{(2)}(u^{n+1}). \tag{1.2}$$

Two-derivative schemes are not restricted to second-order schemes. By adding stages or steps one can obtain orders of accuracy larger than two, like the two-derivative predictor-corrector methods of fourth and sixth-order accuracy that we use for the numerical results [26].

For the CH equation (1.1), the total free energy

$$E(u) := \int_\Omega \left(\frac{\varepsilon^2}{2} \|\nabla u\|^2 + \Phi(u) \right) \mathrm{d}x \tag{1.3}$$

is dissipated, i.e., $E(u(t))$ is a monotonically decreasing function in time t for the exact solution u to Equation (1.1) [15]. This property of the Cahn-Hilliard equation is of utmost importance; it is hence desirable that a numerical integration scheme mimics this behavior. Schemes preserving numerical variants of this energy (energy-stable schemes) have been presented in literature, beginning with the seminal work of Eyre [13], with origins that can be traced back to Elliott and Stuart [12]. For other works on energy stability of the Cahn-Hilliard equation, we refer to [7, 9, 10, 11, 16, 22, 30, 31, 32, 35, 36, 37, 38, 39, 40].

Developing energy-stable schemes is far from being trivial, in particular for high-order schemes. To our knowledge, in this work, we are the first to *show energy stability for a temporal discretization of the Cahn-Hilliard equation using a multiderivative approach*. More precisely, we show that the semi-discretization of Equation (1.1) using the second order Taylor method (1.2), equipped with suitable stability terms inspired by the work of [38], is energy stable for well-chosen parameters. Numerical results demonstrate this behavior, but also show that even without stabilization, the scheme remains energy stable.

Following, we also show higher-order (higher than two) results using the Hermite-Birkhoff predictor-corrector methods that were first developed in [25] and [26]. These methods have shown to be efficient for unsteady PDEs, see [41, 42] and have shown good stability properties [43]. High-order accuracy comes from the correction steps in these methods. We demonstrate that this yields very rapidly converging solutions. Additionally, these schemes are all found to be energy stable in the numerical results.

The paper is organized as follows. In Section 2, we present the stabilized two-derivative implicit Taylor method and we prove the energy stability of the novel method. We also present the numerical findings of the Cahn-Hilliard equation using the novel two-derivative method. We present results concerning the convergence order and the energy stability of the method and how the choice of the stabilization terms influence the method. In Section 3, we present the Hermite-Birkhoff predictor-corrector methods and we present the numerical findings concerning the convergence and the energy stability of the methods. Finally, in Section 4, we present a conclusion and an outlook for this paper.

2 Two-derivative energy stable method

In this section, we consider the semi-discretization in time of Equation (1.1) through the second-order Taylor scheme (1.2). A straightforward computation of the second-order temporal derivatives results in the method

$$u^{n+1} = u^n + \Delta t u_t^{n+1} - \frac{\Delta t^2}{2} u_{tt}^{n+1}, \tag{2.1}$$

with the auxiliary quantities defined as

$$\begin{aligned} u_t^{n+1} &= \Delta\mu^{n+1}, \qquad \mu^{n+1} = \Phi'(u^{n+1}) \qquad -\varepsilon^2\Delta u^{n+1}, \\ u_{tt}^{n+1} &= \Delta\mu_t^{n+1}, \qquad \mu_t^{n+1} = \Phi''(u^{n+1})u_t^{n+1} - \varepsilon^2\Delta u_t^{n+1}. \end{aligned}$$

As usual, we assume that $t^n := n\Delta t$ for $n \in \mathbb{N}$, and u^n denotes an approximation to $u(t^{n+1})$. In order to show the stability of this scheme, inspired by [38] we introduce stability terms into the update of u, Equation (2.1), and the definition of μ. The scheme then reads:

DEFINITION 1 [Stabilized second-order Taylor for CH]. The semi-discrete-in-time stabilized second order Taylor method for Equation (1.1) is given by

$$u^{n+1} = u^n + \Delta t u_t^{n+1} - \frac{\Delta t^2}{2}u_{tt}^{n+1} - \frac{\Delta t^3}{2}a_1\Delta^2\mu^{n+1}, \tag{2.2}$$

with the auxiliary stabilized quantities defined as

$$\begin{aligned} u_t^{n+1} &= \Delta\mu^{n+1}, \qquad \mu^{n+1} = \Phi'(u^{n+1}) \qquad -\varepsilon^2\Delta u^{n+1} + a_2\Delta t(u^{n+1} - u^n), \\ u_{tt}^{n+1} &= \Delta\mu_t^{n+1}, \qquad \mu_t^{n+1} = \Phi''(u^{n+1})u_t^{n+1} - \varepsilon^2\Delta u_t^{n+1}. \end{aligned}$$

Here, a_1 and a_2 denote positive stabilization parameters. Restrictions on the parameters will be obtained from Theorem 1.

Remark 1. Given that a_1 and a_2 are constant values, the scheme presented in Def. 1 is still second order in time, so in this sense, our modifications preserve the order of the Taylor scheme. This can be seen from the fact that the stabilization terms enter to $\mathcal{O}(\Delta t^3)$, as there holds

$$\begin{aligned} \frac{\Delta t^3}{2}a_1\Delta^2\mu^{n+1} &= a_1\Delta t^3\mathcal{O}(1) = \mathcal{O}(\Delta t^3), \\ a_2\Delta t(u^{n+1} - u^n) &= \mathcal{O}(\Delta t)\mathcal{O}(\Delta t) = \mathcal{O}(\Delta t^2). \end{aligned}$$

The latter term occurs in the definition of μ and is in the final update step hence multiplied with an extra Δt.

In the following Subsection 2.1, we prove the energy stability of the stabilized two-derivative implicit Taylor scheme. Afterwards in Subsection 2.2, we investigate the novel method numerically.

2.1 Energy stability

In this section we will prove that the method described in Definition 1 is energy stable under restrictions on the stabilization parameters a_1 and a_2.

Theorem 1. *If the stabilization parameters a_1, a_2 are such that*

$$a_1\Delta t \geq 1, \qquad a_2\Delta t \geq \frac{1}{2}, \tag{2.3}$$

then the time-stepping scheme from Definition 1 is energy stable in the sense that $E(u^{n+1}) \leq E(u^n)$.

Proof. Consider the discretization given in Definition 1, where u_t^{n+1} and μ_t^{n+1} are replaced by their respective definitions. This yields

$$u^{n+1} - u^n = \Delta t \Delta \mu^{n+1} - \frac{\Delta t^2}{2}\left(\Delta\left(\Phi''\left(u^{n+1}\right)\Delta\mu^{n+1}\right) - \varepsilon^2\Delta^3\mu^{n+1}\right) - \frac{\Delta t^3}{2}a_1\Delta^2\mu^{n+1}.$$

Let us define the L^2 inner product in a standard way as $(f,g) := \int_\Omega fg\mathrm{d}x$. We test the equations for u^{n+1} and μ^{n+1} by generic functions q and v to obtain

$$\begin{aligned}\left(u^{n+1} - u^n, q\right) &= \Delta t\left(\Delta\mu^{n+1}, q\right) - \frac{\Delta t^2}{2}\left(\Delta\left(\Phi''\left(u^{n+1}\right)\Delta\mu^{n+1}\right), q\right) \\ &\quad + \frac{\Delta t^2}{2}\varepsilon^2\left(\Delta^3\mu^{n+1}, q\right) - \left(\frac{\Delta t^3}{2}a_1\Delta^2\mu^{n+1}, q\right), \\ \left(\mu^{n+1}, v\right) &= \left(\Phi'\left(u^{n+1}\right), v\right) - \varepsilon^2\left(\Delta u^{n+1}, v\right) + a_2\Delta t(u^{n+1} - u^n, v).\end{aligned}$$

Upon integration by parts, we obtain

$$\begin{aligned}\left(u^{n+1} - u^n, q\right) &= -\Delta t\left(\nabla\mu^{n+1}, \nabla q\right) - \frac{\Delta t^2}{2}\left(\Phi''\left(u^{n+1}\right)\Delta\mu^{n+1}, \Delta q\right) \\ &\quad - \frac{\Delta t^2}{2}\varepsilon^2\left(\nabla\Delta\mu^{n+1}, \nabla\Delta q\right) - \left(\frac{\Delta t^3}{2}a_1\Delta\mu^{n+1}, \Delta q\right), \\ \left(\mu^{n+1}, v\right) &= \left(\Phi'\left(u^{n+1}\right), v\right) + \varepsilon^2\left(\nabla u^{n+1}, \nabla v\right) + a_2\Delta t(u^{n+1} - u^n, v).\end{aligned}$$

Now, take the specific test functions $q := \mu^{n+1}$ and $v := u^{n+1} - u^n$, and insert them into the equation above to get

$$\begin{aligned}\left(u^{n+1} - u^n,\ \mu^{n+1}\right) &= -\Delta t\|\nabla\mu^{n+1}\|^2 - \frac{\Delta t^2}{2}\left(\left(\Phi''\left(u^{n+1}\right)\right)\Delta\mu^{n+1}, \Delta\mu^{n+1}\right) \\ &\quad - \frac{\Delta t^2}{2}\varepsilon^2\left\|\nabla\Delta\mu^{n+1}\right\|^2 - \frac{\Delta t^3}{2}a_1\|\Delta\mu^{n+1}\|^2 \qquad (2.4)\end{aligned}$$

and

$$\begin{aligned}\left(\mu^{n+1},\ u^{n+1} - u^n\right) &= \left(\Phi'\left(u^{n+1}\right), u^{n+1} - u^n\right) + \varepsilon^2\left(\nabla u^{n+1}, \nabla u^{n+1} - \nabla u^n\right) \\ &\quad + a_2\Delta t\left\|u^{n+1} - u^n\right\|^2. \qquad (2.5)\end{aligned}$$

Upon subtracting Equation (2.5) from Equation (2.4) we obtain

$$\begin{aligned}0 = &-\Delta t\left\|\nabla\mu^{n+1}\right\|^2 - \frac{\Delta t^2}{2}\left(\Phi''\left(u^{n+1}\right)\Delta\mu^{n+1}, \Delta\mu^{n+1}\right) - \frac{\Delta t^2}{2}\varepsilon^2\left\|\nabla\Delta\mu^{n+1}\right\|^2 \\ &- \frac{\Delta t^3}{2}a_1\|\Delta\mu^{n+1}\|^2 - \left(\Phi'\left(u^{n+1}\right), u^{n+1} - u^n\right) \\ &- \varepsilon^2\left(\nabla u^{n+1}, \nabla u^{n+1} - \nabla u^n\right) - a_2\Delta t\left\|u^{n+1} - u^n\right\|^2.\end{aligned}$$

We use the identity

$$(a, a-b) = \frac{1}{2}[a^2 - b^2 + (a-b)^2]$$

for the penultimate term $\left(\nabla u^{n+1}, \nabla u^{n+1} - \nabla u^n\right)$ and the Taylor expansion

$$\Phi(u^n) = \Phi(u^{n+1}) - \Phi'(u^{n+1})(u^{n+1} - u^n) + \frac{\Phi''(\xi)}{2}\|u^{n+1} - u^n\|^2$$

with some $\xi \in (u^n, u^{n+1})$ for the term $\left(\Phi'\left(u^{n+1}\right), u^{n+1} - u^n\right)$. This yields

$$\begin{aligned}
0 = &- \Delta t \left\|\nabla \mu^{n+1}\right\|^2 - \frac{\Delta t^2}{2}\left(\Phi''\left(u^{n+1}\right)\Delta\mu^{n+1}, \Delta\mu^{n+1}\right) - \frac{\Delta t^2}{2}\varepsilon^2\left\|\nabla\Delta\mu^{n+1}\right\|^2 \\
&- \frac{\Delta t^3}{2}a_1\|\Delta\mu^{n+1}\|^2 + \int_\Omega \Phi\left(u^n\right)dx - \int_\Omega \Phi\left(u^{n+1}\right)dx - \frac{\Phi''(\xi)}{2}\left\|u^{n+1} - u^n\right\|^2 \\
&- \frac{\varepsilon^2}{2}\left(\left\|\nabla u^{n+1}\right\|^2 - \left\|\nabla u^n\right\|^2 + \left\|\nabla u^{n+1} - \nabla u^n\right\|^2\right) - a_2\Delta t\left\|u^{n+1} - u^n\right\|^2.
\end{aligned}$$

Gathering the energy terms, see (1.3), this can be further simplified to yield

$$\begin{aligned}
0 = &- \Delta t \left\|\nabla \mu^{n+1}\right\|^2 - \frac{\Delta t^2}{2}\left(\Phi''\left(u^{n+1}\right)\Delta\mu^{n+1}, \Delta\mu^{n+1}\right) \\
&- \frac{\Delta t^2}{2}\varepsilon^2\left\|\nabla\Delta\mu^{n+1}\right\|^2 - \frac{\Delta t^3}{2}a_1\|\Delta\mu^{n+1}\|^2 + E\left(u^n\right) - E\left(u^{n+1}\right) \\
&- \frac{\Phi''(\xi)}{2}\left\|u^{n+1} - u^n\right\|^2 - \frac{\varepsilon^2}{2}\left\|\nabla u^{n+1} - \nabla u^n\right\|^2 - a_2\Delta t\left\|u^{n+1} - u^n\right\|^2,
\end{aligned}$$

which means that

$$\begin{aligned}
E(u^{n+1}) - E\left(u^n\right) = &-\Delta t \left\|\nabla \mu^{n+1}\right\|^2 - \frac{\Delta t^2}{2}\left(\Phi''\left(u^{n+1}\right)\Delta\mu^{n+1}, \Delta\mu^{n+1}\right) \\
&- \frac{\Delta t^3}{2}a_1\|\Delta\mu^{n+1}\|^2 - \frac{\Delta t^2}{2}\varepsilon^2\left\|\nabla\Delta\mu^{n+1}\right\|^2 - \frac{\Phi''(\xi)}{2}\left\|u^{n+1} - u^n\right\|^2 \\
&- \frac{\varepsilon^2}{2}\left\|\nabla u^{n+1} - \nabla u^n\right\|^2 - a_2\Delta t\left\|u^{n+1} - u^n\right\|^2.
\end{aligned}$$

Dropping the negative terms, one obtains

$$\begin{aligned}
E(u^{n+1}) - E\left(u^n\right) \le &- \frac{\Delta t^2}{2}\left(\Phi''\left(u\right)\Delta\mu^{n+1}, \Delta\mu^{n+1}\right) - \frac{\Phi''(\xi)}{2}\left\|u^{n+1} - u^n\right\|^2 \\
&- \frac{\Delta t^3}{2}a_1\|\Delta\mu^{n+1}\|^2 - a_2\Delta t\left\|u^{n+1} - u^n\right\|^2. \qquad (2.6)
\end{aligned}$$

For the double-well potential, there holds $\Phi''(u) = 3u^2 - 1$, and hence

$$\Phi''(u) \ge -1.$$

Therefore, Equation (2.6) can be written as

$$\begin{aligned}
E\left(u^{n+1}\right) - E\left(u^n\right) \le &\frac{\Delta t^2}{2}\|\Delta\mu^{n+1}\|^2 + \frac{1}{2}\left\|u^{n+1} - u^n\right\|^2 \\
&- \frac{\Delta t^3}{2}a_1\left\|\Delta\mu^{n+1}\right\|^2 - a_2\Delta t\left\|u^{n+1} - u^n\right\|^2.
\end{aligned}$$

The right-hand side is negative if there holds

$$1 - a_1 \Delta t \leq 0, \qquad \frac{1}{2} - a_2 \Delta t \leq 0,$$

which indeed yields the restrictions (2.3) as stated in the theorem. □

Remark 2. Let us mention that the result shown here is somehow suboptimal. First of all, we are not able to obtain unconditional stability in Δt. There is the somewhat counterintuitive restriction that, as smaller Δt gets, the more stabilization one needs to add. We will point out in our numerical results that we cannot observe such a behavior numerically. Second, one might be tempted to choose the stability coefficients as $\mathcal{O}(\Delta t^{-1})$. However, then one would loose an order of accuracy. To fulfill the conditions of Theorem 1 and at the same time keep the second-order accuracy of the scheme, one can keep a_1 and a_2 fixed, but only consider Δt large enough to fulfill the constraints (2.3). However, in practice, a_1 and a_2 are chosen and kept constant over the whole range of Δt considered, even if the restrictions from Theorem 1 are violated. Numerically, it will be seen that this is a reasonable choice.

2.2 Numerical findings

In this section, we present numerical findings on the stabilized method, including a study on the influence of the stability parameters a_1 and a_2. The one-dimensional version of Equation (1.1) is used. The algorithm from Definition 1 is implemented in its primal form, meaning that the definitions of μ and μ_l are inserted into u and u_l, respectively. Hence, we use the following straightforward three and five-point central finite difference discretizations for the second and the fourth-order spatial derivative, respectively:

$$\partial_x^2 u_i \approx \frac{u_{i-1} - 2u_i + u_{i+1}}{\Delta x^2},$$
$$\partial_x^4 u_i \approx \frac{u_{i-2} - 4u_{i-1} + 6u_i - 4u_{i+1} + u_{i+2}}{\Delta x^4}.$$

In all cases, Δx denotes the spatial step size; u_i denotes u at spatial position $x_i := i\Delta x$. At the boundaries, the finite difference is changed to incorporate the homogeneous Neumann conditions on u and μ.[1] With this choice of spatial discretization and boundary conditions, the scheme is globally mass conservative in the sense that $\int_\Omega u dx$ is constant in time.

For Cahn-Hilliard, there are hardly any exact solutions (for some attempts, consider [33]). In this work, we are interested in temporal integration, which is why we use Matlab's ode15s solver at a very fine error tolerance of 10^{-16} to integrate the semi-discrete (in space) Cahn-Hilliard equations; thereby obtaining a reference solution. It is important to note that we do not include stabilization terms into this computation. As error measure, we then use the quantity

$$e := \|u^N - u(T_{\text{end}})\|_2,$$

[1] Please note that in one dimension, it is easy to see that when $\partial_x \mu = 0$ this leads to $\partial_x^3 u = 0$ due to the definition of μ.

where $N := \frac{T_{\text{end}}}{\Delta t}$, u^N is the approximate solution at time $t^N \equiv T_{\text{end}}$, and u is the "exact" reference solution.

For simplicity, we consider the 1D Cahn-Hilliard equation on the domain $\Omega = [-5, 5]$ with different values for the thickness interface $\varepsilon = \sqrt{0.1}$ and $\varepsilon = 0.1$.

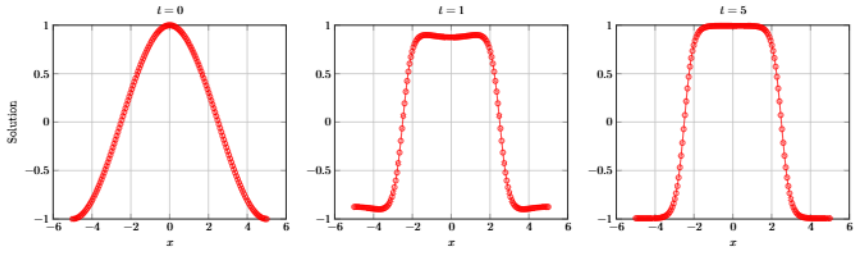

Figure 1. The reference solution of 1D Cahn-Hilliard equation for different times $t = 0$, $t = 1$, and $t = 5$, with interface thickness $\varepsilon = \sqrt{0.1}$ in spatial domain $\Omega = [-5, 5]$. Initial condition is given by Equation (2.7).

Figure 1 shows the evolution of the Cahn-Hilliard equation for an interface thickness of $\varepsilon = \sqrt{0.1}$ and initial condition

$$u(x, 0) = \cos\left(\frac{\pi x}{5}\right). \tag{2.7}$$

The time frames are at three time instances $t = 0$, $t = 1$ and $t = 5$, respectively. The reference solution on a spatial grid with 155 elements using the Matlab "ode15s" routine is shown. The typical 'phase-separation' is observed in the solution.

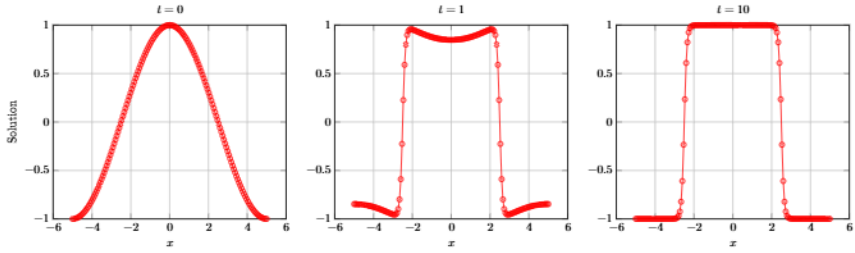

Figure 2. The reference solution of 1D Cahn-Hilliard equation for different times $t = 0$, $t = 1$, and $t = 10$, with interface thickness $\varepsilon = 0.1$ in spatial domain $\Omega = [-5, 5]$. Initial condition is given by Equation (2.7).

Figure 2 shows the evolution of the reference solution of the Cahn-Hilliard equation for a sharper interface thickness of $\varepsilon = 0.1$ and same initial conditions and spatial grid as before. The time frames are at three time instances $t = 0$, $t = 1$ and $t = 10$, respectively. We see that the interface is sharper than before, as expected, and it needs more time to separate the phases.

Smaller values of ε would require finer spatial grid and finer time-step size to be stable. This is however common for the Cahn-Hilliard equation. The spatial mesh is formed of $N = 155$ elements to ensure that the error from the spatial discretization will not dominate. For the numerical results, the final time is $T_{\text{end}} = 1.0$ for $\varepsilon = \sqrt{0.1}$, and $\varepsilon = 0.1$. For the convergence plots we double the number of timesteps in every refinement. The convergence rates are shown on a logarithmic scale. It is worth noting that we focus on the convergence and the accuracy *in time* and not in space. Therefore, only the time-step size is refined. For the nonlinear solver, we use Newton's method with relative and absolute tolerance at 10^{-12}. The stabilization terms a_1 and a_2 are chosen according to Theorem 1. We use Δt at the finest refinement of the convergence plots to choose appropriate values for the coefficients a_1 and a_2.

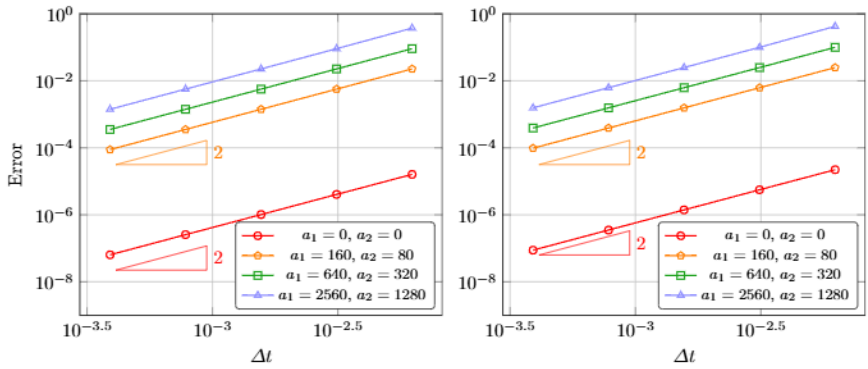

Figure 3. Convergence plots of the implicit two-derivative Taylor method using different stabilization terms with parameters $T_{\text{end}} = 1.0$, $\varepsilon = \sqrt{0.1}$ (left) and $\varepsilon = 0.1$ (right) in space domain $\Omega = [-5, 5]$.

In Figure 3, convergence plots for both $\varepsilon = \sqrt{0.1}$ and $\varepsilon = 0.1$ are shown for the unstabilized and the stabilized (with different stabilization parameters) two-derivative implicit Taylor method. We observe that the scheme for every choice of the stabilization terms a_1 and a_2 achieves the expected second-order. In addition, it can be observed that the errors are higher when the stabilization parameters are larger. This is something that, at least as as long as the computations remain stable, was to be expected. The larger a_1 and a_2, the more 'inconsistencies' are introduced in Equation (2.2), hence the worse the accuracy is.

To confirm the results of Theorem 1, the energy is plotted in Figure 4. It can be clearly seen that there is energy dissipation for both choices of ε and all choices of the stabilization parameters – but also for the unstabilized variant. For the larger ε, differences are negligible, while for the smaller ε, one can clearly see some minor differences. To conclude, we can confirm the results from Theorem 1. However, we also see that the stabilization terms are not really necessary, which we have confirmed for other initial conditions, not

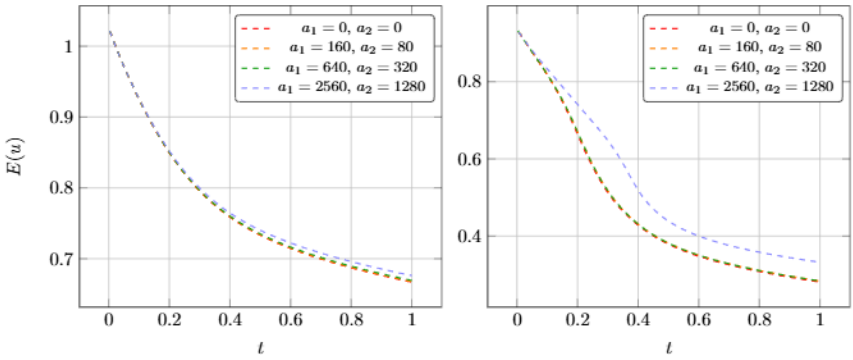

Figure 4. Energy for the two-derivative implicit Taylor method with different choices of stabilization terms and parameters $\varepsilon = \sqrt{0.1}$ (left) and $\varepsilon = 0.1$ (right) in spatial domain $\Omega = [-5, 5]$.

shown here, as well. Hence, in the next section, we will apply higher-order two-derivative methods to the problem at hand without stabilization.

3 Higher-order time integration

The Hermite-Birkhoff predictor-corrector method (HBPC for short) has been introduced in [25] and extended in [27], originally for applications that required implicit/explicit splittings. The method has been discussed in detail in [27], so we will only shortly review it here. The method computes an initial aproximation $u^{n,[0]}$ to the exact solution at time t^{n+1}, and then subsequently corrects it to obtain higher-order approximations $u^{n,[k]}$. We have chosen this method as its intermediate steps closely resemble the second-order Taylor method.

The method needs a background two-derivative Runge-Kutta scheme, represented through its Butcher tableaux for the first- and second-order derivative, respectively, $A^{(1)}_{lj}$ and $A^{(2)}_{lj}$, for $1 \le l \le s$, where s denotes the number of stages. In this work, we use the fourth- and sixth-order schemes presented in [27, (2) and (3)], respectively.

Given that $Q(u)$ is an approximation to the primal Cahn-Hilliard operator $\Phi'(u^{n+1})_{xx} - \varepsilon u^{n+1}_{xxxx}$ as discussed in Section 2.2, the HBPC algorithm can be formulated as follows:

Algorithm 1 (HBPC($q, k_{\max}$)) *In a first step, stage values are predicted using a second-order Taylor scheme; subsequently, these values are corrected towards the background Runge-Kutta scheme.*

1. ***Predict.*** *Solve the following expression for $u^{n,[0],l}$ and for each stage $1 \le l \le s$:*

$$u^{n,[0],l} := u^n + c_l \Delta t Q^{n,[0],l} - \frac{(c_l \Delta t)^2}{2} \dot{Q}^{n,[0],l}.$$

2. ***Correct.*** *The following expression is solved for* $u^{n,[k+1],l}$ *for each* $1 \leq l \leq s$ *and* $0 \leq k \leq k_{\max} - 1$*:*

$$u^{n,[k+1],l} := u^n + \Delta t \left(Q^{n,[k+1],l} - Q^{n,[k],l} \right) - \frac{\Delta t^2}{2} \left(\dot{Q}^{n,[k+1],l} - \dot{Q}^{n,[k],l} \right) + \mathcal{I}_l(Q^{n,[k],0}, \ldots, Q^{n,[k],s}).$$

3. ***Update.***

$$u^{n+1} := u^{n,[k_{\max}],s},$$

where $\mathcal{I}_l$ is the underlying Runge-Kutta quadrature rule which is only computed explicitly, and the approximation of the solution is denoted as $u^{n,[k],l} \approx u(t^n + c_l \Delta t)$. Also, for simplicity in notation we omit the u of the symbolism $Q(u)$ in prediction and correction step. For example, instead of $Q(u^{n,[0],l})$ we use the notation $Q^{n,[0],l}$. For the numerical results we use two types of the method HBPC$(q, k_{\max})$, one with $q = 4$ and two stages and one with $q = 6$ and three stages; see again [27, (2) and (3)].

3.1 Numerical findings

In this section, we investigate the accuracy and energy stability of the HBPC $(q, k_{\max})$ methods mentioned before in Algorithm 1 numerically. We keep the same parameters of the example problem as in Section 2.2. The spatial mesh is formed of $N = 155$ elements with the same initial condition (2.7) and using the same spatial discretization method. For the numerical results, the final time of the simulation for $\varepsilon = \sqrt{0.1}$ is $T_{\text{end}} = 3.0$. In order to see the relatively high order of the schemes HBPC$(q, k_{\max})$, we have extended the final time to $T_{\text{end}} = 3$ for this simulation. For $\varepsilon = 0.1$ the final time remained $T_{\text{end}} = 1.0$. We refine only the time-step size and not the spatial grid as before. For the nonlinear solver, we use Newton's method with relative and absolute tolerance of 10^{-12}.

It is important to note that for all the numerical results we obtain in this section, the stabilization coefficients a_1 and a_2 are set to zero. This is because we have observed in Section 2.2 that the energy stability is maintained even if we violate the conditions of Theorem 1. For the HBPC methods we use the necessary number of the correction steps to achieve the proper order. Hence, for the method HBPC(4,2) we use $k_{\max} = 2$ and for HBPC(6,4) we use $k_{\max} = 4$ which are the minimum correction steps to obtain the expected order of the HBPC methods.

In Figure 5 on the left we see convergence for all three methods for interface thickness $\varepsilon = \sqrt{0.1}$. On the right the convergence rates are shown for $\varepsilon = 0.1$. We can see that the orders of accuracy are met in both cases. In the left plot for the HBPC methods we observe that the errors stay around the Newton tolerance.

In Figure 6, we can see the convergence plots for the two Hermite-Birkhoff predictor-corrector methods HBPC(4,$k_{\max}$) on the left and HBPC(6,$k_{\max}$) on the right, with interface thickness set to $\varepsilon = \sqrt{0.1}$ and for different values of

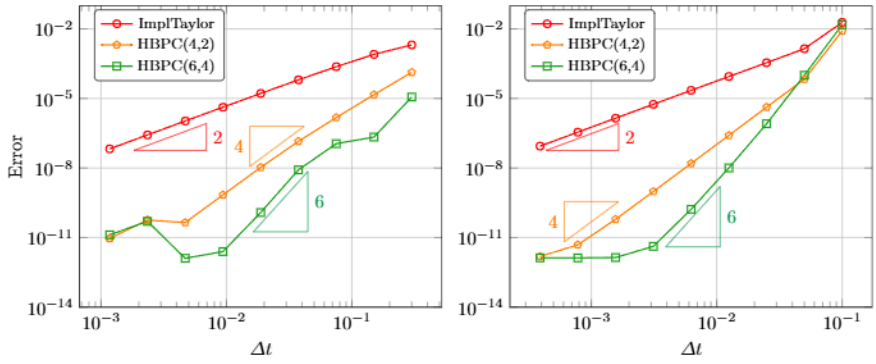

Figure 5. Convergence plots for all methods without stabilization terms and parameters $T_{\text{end}} = 3.0$, $\varepsilon = \sqrt{0.1}$ (left) and $T_{\text{end}} = 1.0$, $\varepsilon = 0.1$ (right) in space domain $\Omega = [-5, 5]$.

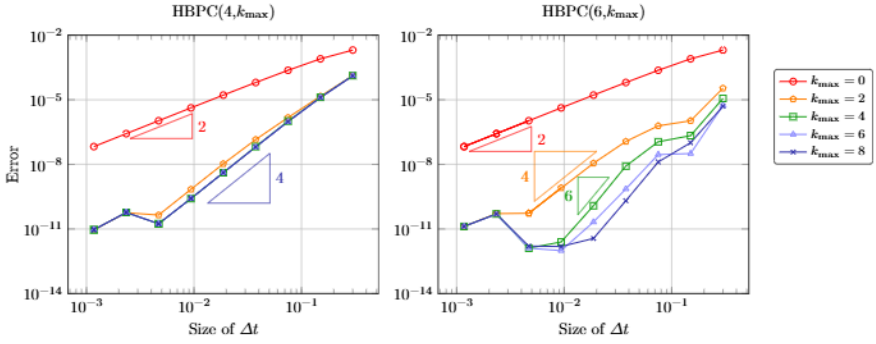

Figure 6. Convergence plots for the methods HBPC(4,$k_{\max}$) (left) and HBPC(6,$k_{\max}$) (right) without stabilization terms and parameters $T_{\text{end}} = 3.0$, $\varepsilon = \sqrt{0.1}$ and different amount of correction steps in space domain $\Omega = [-5, 5]$.

correction steps. We can see the influence of $k_{\max}$ values on the error. First, when $k_{\max} = 0$, we observe a second-order accuracy because the predictor is a two-derivative implicit scheme. After two correction steps, we observe a fourth order of accuracy, the maximum for the HBPC(4,$k_{\max}$) method. After four correction steps, the HBPC(6,$k_{\max}$) can achieve the maximum sixth-order convergence. In the left plot, we can see that for $k_{\max} = 4, 6, 8$, the error does not decrease any more. On the other hand, with the method HBPC(6,$k_{\max}$), we can see that the error keeps decreasing very close to the Newton tolerance without any time refinement for all number of correction steps.

In Figure 7, we see the convergence plots for the two Hermite-Birkhoff predictor-corrector methods HBPC(4,$k_{\max}$) on the left and HBPC(6,$k_{\max}$) on the right, with smaller interface thickness $\varepsilon = 0.1$ and for different values of correction steps. We observe similar behavior as in the case that $\varepsilon = \sqrt{0.1}$. Therefore, the increased stiffness does not affect the behavior of the method. The reason for the fact that the error stops decreasing around 10^{-10} to 10^{-12}

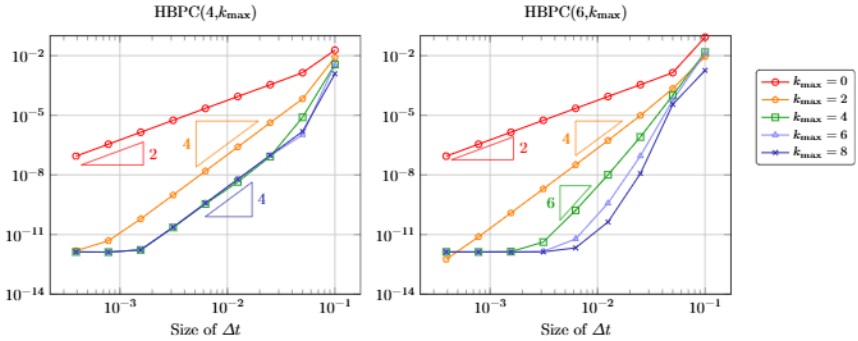

Figure 7. Convergence plots for the methods HBPC(4,$k_{\max}$) (left) and HBPC(6,$k_{\max}$) (right) without stabilization terms and parameters $T_{\text{end}} = 1.0$, $\varepsilon = 0.1$ and different amount of correction steps in space domain $\Omega = [-5, 5]$.

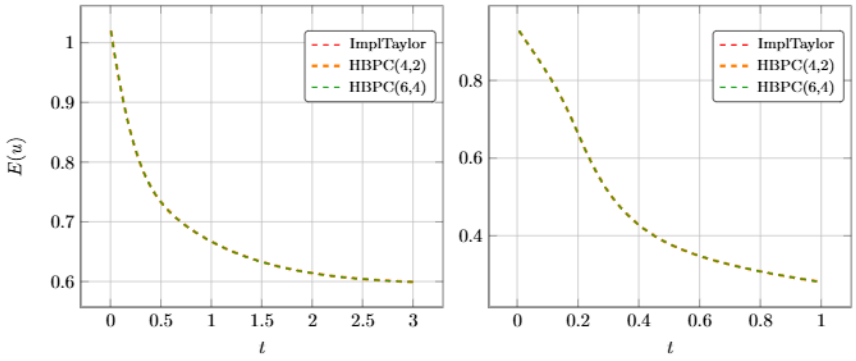

Figure 8. Energy for all three methods without stabilization terms and $\varepsilon = \sqrt{0.1}$ (left) and $\varepsilon = 0.1$ (right) in space domain $\Omega = [-5, 5]$. Note that the three lines stand on top of each other.

in Figures 5, 6 and 7 is attributed to the finite Newton tolerance of 10^{-12}.

Finally, we present numerical findings regarding the energy stability. In all the cases that we present here, there is energy dissipation, see Figure 8, although there are no stabilization terms. We can see that the results are very similar compared to Figure 4 where energy for stabilized two-derivative Taylor method is shown. There is not a strong influence of the time discretization methods or the absence of the stabilization terms in the energy. We notice that all methods exhibit energy dissipation even when we violate the conditions of Theorem 1.

4 Conclusions and outlook

We have presented a novel second-order implicit Taylor method that maintains the energy stability of the Cahn-Hilliard equation. We showed numerically

that the second-order Taylor method is energy stable even without stabilization terms. The second-order convergence was achieved in any case. We showed that the choice of different stabilization parameters did not influence the order of the method, but had an influence on the size of the error. We observed that the error was larger when we chose larger values of stabilization parameters. In addition, we performed numerical experiments with two more two-derivative methods, a fourth and a sixth-order Hermite-Birkhoff predictor-corrector method. We observed that the expected orders were achieved in all cases, and the energy stability was maintained. Regarding the energy stability we observed energy dissipation in all cases, even in the cases that the bounds of the stabilization parameters were violated. In addition we noticed that the energy was influenced by the interface thickness ε and by the size of the stabilization parameters, but not by the choice of the time discretization method.

Future work focuses on extending the methodology shown here to methods with more than two derivatives. This will pose extra challenges, as each additional temporal derivative influence the stiffness of the problem negatively. Furthermore, the ultimate goal is a parameter-free energy-stable scheme of uniform high order. In this sense, the current work represents an important step.

Acknowledgements

E. Theodosiou was funded by the Fonds voor Wetenschappelijk Onderzoek (FWO, Belgium) - project no. G052419N.

References

[1] A. Abdi, G. Hojjati and M. Sharifi. Implicit–explicit second derivative diagonally implicit multistage integration methods. *Computational and Applied Mathematics*, **39**(3), 2020. https://doi.org/10.1007/s40314-020-01252-1.

[2] V.E. Badalassi, H.D. Ceniceros and S. Banerjee. Computation of multiphase systems with phase field models. *Journal of Computational Physics*, **190**(2):371–397, 2003. https://doi.org/10.1016/S0021-9991(03)00280-8.

[3] F. Bai, X. He, X. Yang, R. Zhou and C. Wang. Three dimensional phase-field investigation of droplet formation in microfluidic flow focusing devices with experimental validation. *International Journal of Multiphase Flow*, **93**:130–141, 2017. https://doi.org/10.1016/j.ijmultiphaseflow.2017.04.008.

[4] A.R. Balakrishna and C.W. Carter. Combining phase-field crystal methods with a Cahn-Hilliard model for binary alloys. *Physical Review E*, **97**(4):043304, 2018. https://doi.org/10.1103/PhysRevE.97.043304.

[5] M. Biskup, L. Chayes and R. Kotecký. On the formation/dissolution of equilibrium droplets. *Europhysics Letters*, **60**(1):21–27, 2002. https://doi.org/10.1209/epl/i2002-00312-y.

[6] J.W. Cahn and J.E. Hilliard. Free energy of a nonuniform system. I. Interfacial free energy. *J. Chem. Phys.*, **28**(2):258–267, 1958. https://doi.org/10.1063/1.1744102.

[7] K. Cheng, C. Wang, S.M. Wise and X. Yue. A Second-Order, Weakly Energy-Stable Pseudo-spectral Scheme for the Cahn–Hilliard Equation and its Solution by the Homogeneous Linear Iteration Method. *J. Sci. Comput.*, **69**(3):1083–1114, 2016. https://doi.org/10.1007/s10915-016-0228-3.

[8] L. Cherfils, A. Miranville and S. Zelik. On a generalized Cahn-Hilliard equation with biological applications. *Discrete and Continuous Dynamical Systems - B*, **19**(7):2013–2026, 2014. https://doi.org/10.3934/dcdsb.2014.19.2013.

[9] A.E. Diegel, C. Wang, X. Wang and S.M. Wise. Convergence analysis and error estimates for a second order accurate finite element method for the Cahn–Hilliard–Navier–Stokes system. *Numer. Math.*, **137**(3):495–534, 2017. https://doi.org/10.1007/s00211-017-0887-5.

[10] A.E. Diegel, C. Wang and S.M. Wise. Stability and Convergence of a Second Order Mixed Finite Element Method for the Cahn-Hilliard Equation. *Communications in Mathematical Sciences*, **14**(2), 2014. Available on Internet: `https://arxiv.org/pdf/1411.5248.pdf`

[11] L. Dong, C. Wang, S.M. Wise and Z. Zhang. A positivity-preserving, energy stable scheme for a ternary Cahn-Hilliard system with the singular interfacial parameters. *Journal of Computational Physics*, **442**:110451, 2021. https://doi.org/10.1016/j.jcp.2021.110451.

[12] C.M. Elliott and A.M. Stuart. The global dynamics of discrete semilinear parabolic equations. *SIAM Journal on Numerical Analysis*, **30**(6):1622–1663, 1993. https://doi.org/10.1137/0730084.

[13] D.J. Eyre. Unconditionally gradient stable time marching the Cahn-Hilliard equation. *MRS Online Proceedings Library*, **529**:39, 1998. https://doi.org/10.1557/PROC-529-39.

[14] H. Fakih. A Cahn–Hilliard equation with a proliferation term for biological and chemical applications. *Asymptotic Analysis*, **94**(1-2):71–104, 2015. https://doi.org/10.3233/asy-151306.

[15] V.L. Ginzburg. On the theory of superconductivity. *Il Nuovo Cimento (1955-1965)*, **2**:1234–1250, 1955. https://doi.org/10.1007/BF02731579.

[16] J. Guo, C. Wang, S.M. Wise and X. Yue. An H^2 convergence of a second-order convex-splitting, finite difference scheme for the three-dimensional Cahn–Hilliard equation. *Communications in Mathematical Sciences*, **14**(2):489–515, 2016. https://doi.org/10.4310/cms.2016.v14.n2.a8.

[17] R. Guo and Y. Xu. Efficient solvers of discontinuous Galerkin discretization for the Cahn–Hilliard equations. *J. Sci. Comput.*, **58**(2):380–408, 2013. https://doi.org/10.1007/s10915-013-9738-4.

[18] E. Hairer and G. Wanner. Multistep-multistage-multiderivative methods for ordinary differential equations. *Computing*, **11**(3):287–303, 1973. https://doi.org/10.1007/BF02252917.

[19] A. Jaust, J. Schütz and D.C. Seal. Implicit multistage two-derivative discontinuous Galerkin schemes for viscous conservation laws. *J. Sci. Comput.*, **69**:866–891, 2016. https://doi.org/10.1007/s10915-016-0221-x.

[20] J. Kim. Phase-Field Models for Multi-Component Fluid Flows. *Communications in Computational Physics*, **12**(3):613–661, 2012. https://doi.org/10.4208/cicp.301110.040811a.

[21] J. Kim, S. Lee, Y. Choi, S.M. Lee and D. Jeong. Basic principles and practical applications of the Cahn–Hilliard equation. *Mathematical Problems in Engineering*, **2016**:1–11, 2016. https://doi.org/10.1155/2016/9532608.

[22] H.L. Liao, B. Ji, L. Wang and Z. Zhang. Mesh-robustness of an energy stable BDF2 scheme with variable steps for the Cahn–Hilliard model. *J. Sci. Comput.*, **92**(2), 2022. https://doi.org/10.1007/s10915-022-01861-4.

[23] C. Liu, F. Frank and B.M. Rivière. Numerical error analysis for nonsymmetric interior penalty discontinuous Galerkin method of Cahn–Hilliard equation. *Numerical Methods for Partial Differential Equations*, **35**(4):1509–1537, 2019. https://doi.org/10.1002/num.22362.

[24] A. Novick-Cohen. Chapter 4 the Cahn–Hilliard equation. In *Handbook of Differential Equations: Evolutionary Equations*, pp. 201–228. Elsevier, 2008. https://doi.org/10.1016/s1874-5717(08)00004-2.

[25] J. Schütz and D. Seal. An asymptotic preserving semi-implicit multiderivative solver. *Applied Numerical Mathematics*, **160**:84–101, 2021. https://doi.org/10.1016/j.apnum.2020.09.004.

[26] J. Schütz, D.C. Seal and J. Zeifang. Parallel-in-time high-order multiderivative IMEX methods. *J. Sci. Comput.*, **90**(54), 2022. https://doi.org/10.1007/s10915-021-01733-3.

[27] J. Schütz, D.C. Seal and J. Zeifang. Parallel-in-time high-order multiderivative IMEX solvers. *J. Sci. Comput.*, **90**(54):1–33, 2022. https://doi.org/10.1016/j.apnum.2020.09.004.

[28] J. Schütz, D.C. Seal and A. Jaust. Implicit multiderivative collocation solvers for linear partial differential equations with discontinuous Galerkin spatial discretizations. *J. Sci. Comput.*, **73**(2-3):1145–1163, 2017. https://doi.org/10.1007/s10915-017-0485-9.

[29] D.C. Seal, Y. Güçlü and A. Christlieb. High-order multiderivative time integrators for hyperbolic conservation laws. *J. Sci. Comput.*, **60**:101–140, 2014. https://doi.org/10.1007/s10915-013-9787-8.

[30] J. Shen and X. Yang. Numerical approximations of Allen-Cahn and Cahn-Hilliard equations. *Discrete and Continuous Dynamical Systems*, **28**(4):1669–1691, 2010. https://doi.org/10.3934/dcds.2010.28.1669.

[31] H. Song. Energy SSP-IMEX Runge–Kutta methods for the Cahn–Hilliard equation. *Journal of Computational and Applied Mathematics*, **292**:576–590, 2016. https://doi.org/10.1016/j.cam.2015.07.030.

[32] H. Song and C.W. Shu. Unconditional Energy Stability Analysis of a Second Order Implicit–Explicit Local Discontinuous Galerkin Method for the Cahn–Hilliard Equation. *J. Sci. Comput.*, **73**(2-3):1178–1203, 2017. https://doi.org/10.1007/s10915-017-0497-5.

[33] Y. Ugurlu and D. Kaya. Solutions of the Cahn–Hilliard equation. *Computers & Mathematics with Applications*, **56**(12):3038–3045, 2008. https://doi.org/10.1016/j.camwa.2008.07.007.

[34] F.J. Vermolen, A. Segal and A. Gefen. A pilot study of a phenomenological model of adipogenesis in maturing adipocytes using Cahn-Hilliard theory. *Med. Biol. Eng. Comput.*, **49**(12):1447–1457, 2011. https://doi.org/10.1007/s11517-011-0802-7.

[35] L. Wang and H. Yu. Convergence Analysis of an Unconditionally Energy Stable Linear Crank-Nicolson Scheme for the Cahn-Hilliard Equation. *J. Math. Study*, **51**(1):89–114, 2018. https://doi.org/10.4208/jms.v51n1.18.06.

[36] L. Wang and H. Yu. On Efficient Second Order Stabilized Semi-implicit Schemes for the Cahn-Hilliard Phase-Field Equation. *J. Sci. Comput.*, **77**(2):1185–1209, 2018. https://doi.org/10.1007/s10915-018-0746-2.

[37] L. Wang and H. Yu. An energy stable linear diffusive Crank–Nicolson scheme for the Cahn–Hilliard gradient flow. *Journal of Computational and Applied Mathematics*, **377**:112880, 2020. https://doi.org/10.1016/j.cam.2020.112880.

[38] X. Wu, G.J. van Zwieten and K.G. van der Zee. Stabilized second-order convex splitting schemes for Cahn-Hilliard models with application to diffuse-interface tumor-growth models. *International Journal for Numerical Methods in Biomedical Engineering*, **30**(2):180–203, 2013. https://doi.org/10.1002/cnm.2597.

[39] Y. Yan, W. Chen, C. Wang and S.M. Wise. A Second-Order Energy Stable BDF Numerical Scheme for the Cahn-Hilliard Equation. *Communications in Computational Physics*, **23**(2), 2018. https://doi.org/10.4208/cicp.oa-2016-0197.

[40] J. Yang, J. Wang and J. Kim. Energy-stable method for the Cahn–Hilliard equation in arbitrary domains. *International Journal of Mechanical Sciences*, **228**:107489, 2022. https://doi.org/10.1016/j.ijmecsci.2022.107489.

[41] J. Zeifang, A.T. Manikantan and J. Schütz. Time parallelism and Newton-adaptivity of the two-derivative deferred correction discontinuous Galerkin method. *Applied Mathematics and Computation*, **457**:128198, 2023. https://doi.org/10.1016/j.amc.2023.128198.

[42] J. Zeifang and J. Schütz. Implicit two-derivative deferred correction time discretization for the discontinuous Galerkin method. *Journal of Computational Physics*, **464**:111353, 2022. https://doi.org/10.1016/j.jcp.2022.111353.

[43] J. Zeifang, J. Schütz and D. Seal. Stability of implicit multiderivative deferred correction methods. *BIT Numerical Mathematics*, **62**:1487–1503, 2022. https://doi.org/10.1007/s10543-022-00919-x.